A probabilistic approach to predict the very high-cycle fatigue behaviour of spheroidal graphite cast iron structures

Isabelle Chantier, Véronique Bobet, René Billardon, François Hild

A probabilistic approach to predict the very high-cycle fatigue behaviour of spheroidal graphite cast iron structures

I. CHANTIER, V. BOBET,[1] R. BILLARDON and F. HILD*

LMT-Cachan, ENS de Cachan, CNRS, Université Paris 6, 61 avenue du Président Wilson, F-94235 Cachan Cedex, France, [1]*Renault Technocentre, Direction de la Recherche, Service 64230, 1 avenue du Golf, F-78288 Guyancourt, Cedex, France*

ABSTRACT A new probabilistic approach is developed to study structures made of spheroidal graphite cast iron and subjected to very high-cycle fatigue. Until now, the probabilistic approach was based on S–N curves obtained from experiments carried out only until 10^7 cycles. To validate this approach, failure predictions relating to the safety of components are computed and compared to experimental results. In addition to this development, an extension is proposed in order to improve the very long life assessment of complex structures. An extrapolation of the previous fatigue results to 10^9–10^{11} cycles illustrates the error made on cumulative failure probabilities. Finally, the respective influence of the casting flaw distribution, volume and stress field heterogeneity within specimens and industrial components is studied.

Keywords very high-cycle fatigue, probabilistic approach, casting flaw distribution, volume effect, stress heterogeneity effect, surface effect.

NOMENCLATURE

a, a_M = current and maximum flaw size
a_c, a_{c0}, a_{th} = critical, initial critical or threshold flaw size
a_0, a_N = flaw size after 0 or N cycles
$B_{\alpha\beta}$ = Euler function of the first kind
C, n, m = parameters of the crack propagation law
f_0, f_N = initial and current flaw size distributions
g = function modelling the effect of the load ratio
$H^*_{\beta+1}$, $H_{\beta+1}$ = stress heterogeneity factors
K_c, K_{th} = critical and threshold stress intensity factors
K_{min}, K_{max} = minimum and maximum stress intensity factors
N, N_F = number of cycles and cycles to failure, respectively
P_{F0}, P_F = cumulative failure probability of an element and a structure
R = load ratio
S_{th} = threshold stress
V_0, V = volume of an element and a structure
V^*_{eff} = effective volume
W = positive dimensionless parameter
x_{th} = dimensionless stress
Y = geometric dimensionless parameter
α, β = parameters of a beta function
ΔK_{eff} = effective stress intensity range
σ = equivalent stress (e.g. maximum principal stress)
σ_0 = scale parameter
σ_{max}, σ_F = maximum and failure stresses
φ = function
Φ = diameter
Ω_0, Ω = volume element, structure
$\langle \cdot \rangle$ = positive part of

INTRODUCTION

This study is directly related to the efforts made by car manufacturers to improve the life assessment for safe components, e.g. suspension arms, which are made of spheroidal graphite (SG) cast iron and subjected to very high-cycle fatigue (VHCF) loadings. The industrial challenge consists of designing better components that are also cheaper and manufactured faster. To reach this goal in the case of safe cast safety components, the lifing procedures must integrate a fatigue analysis that is reliable enough to avoid tests and the rejection of components, i.e. to reduce the time for design, development and non-destructive testing after the manufacturing process. Structural reliability analyses[1] could be used to evaluate the fatigue life of cast components. However, most of the analyses do not account for the actual cause of failure. In this paper, it is proposed to introduce a mechanism-based probabilistic model.

This study is a first attempt to justify the use of a probabilistic approach for the design of such components up to the gigacycle regime. The fatigue strength of cast parts is generally reduced by the presence of initial casting flaws that are more or less randomly distributed within the material. Under cyclic loading conditions, microcracks propagate from these initial flaws. Finally, macrocrack propagation usually takes place first in a stable and then in an unstable way. However, macrocrack propagation represents only a negligible fraction of the life of components subjected to high- or very high-cycle fatigue loadings. It follows therefore that any approach used to predict very high-cycle fatigue failure should be supported by the weakest link theory.[2] Hence, it is assumed that the components remain macroscopically elastic, and that the microscopic evolution of the initial flaws can be described up to failure by a modified Paris' law. The observation of scattered results on Wöhler diagrams of SG cast iron confirms the need for a probabilistic approach.

In this paper, the material properties are first listed and the framework of the probabilistic approach is then recalled. Secondly, the failure probabilities depending upon stress level and initial flaw size distributions within the components are defined. Thirdly, predictions based on this probabilistic model are analysed and an extrapolation of this approach to the gigacycle regime is proposed. Finally, so-called DVH effects (where D stands for flaw size distribution, V for volume and H for stress heterogeneity)[3] are shown.

THE STUDIED MATERIAL

The %wt composition of the ferritic SG cast iron studied here was: 3.8C, 3.21Si, 0.01Mg, 0.04S and 0.007P with the remainder ferrite. This material contains less than 5% of pearlite. The main microstructural characteristics are: mean graphite nodule diameter = 17 μm, ferritic grain size = 15–22 μm, mean distance between nodules = 80 μm [Fig. 1(a)].[4] For as-cast components, the tensile properties are: yield stress = 360 MPa, ultimate strength = 490 MPa, elongation = 4%, Young's modulus = 150 GPa. Figure 1(b) shows typical casting flaws leading to failure. If these flaws are modelled by cracks that experience stable propagation, the corresponding stress intensity factor can be defined by $K = Y\sigma\sqrt{a}$ and the propagation law by a modified Paris' law[5,6]

$$\frac{da}{dN} = C\,\Delta K_{\text{eff}}^{n} \quad \text{with} \quad \Delta K_{\text{eff}} = \frac{K_{\max}\,g(R) - K_{\text{th}}}{K_c - \dfrac{K_{\text{th}}}{g(R)}} \tag{1}$$

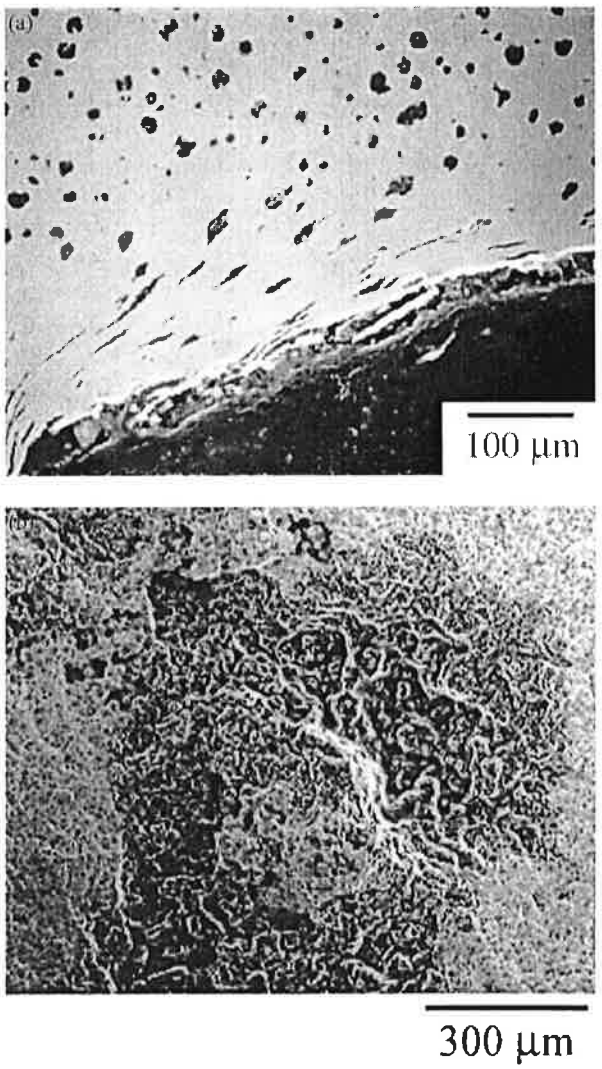

Fig. 1 Typical microstructures of SG cast iron. (a) Graphite nodules in the vicinity of an as-cast surface. (b) A microshrinkage cavity observed on the fatigue fracture surface of a suspension arm.

and

$$g(R) = \frac{1-R}{1-mR} \quad \text{with} \quad R = \frac{K_{\min}}{K_{\max}} \tag{2}$$

In the case of VHCF, $K_{\max} g(R)$ is close to the threshold stress intensity factor K_{th}, for which the non-propagation condition is given by $K_{\max} g(R) < K_{th}$. The criterion for local failure considers that $K_{\max} \geqslant K_c$, and the effective stress intensity range ΔK_{eff} is positive. By using this criterion, one can determine a critical flaw size a_c associated to a stress level $\sigma_{\max}$. By integrating Eq. (1), the number of cycles to failure N_F is found to be a function of the initial flaw size a_{c0}, the maximum flaw size a_M, the load ratio R, the fatigue limit for a volume element with the largest flaw size S_{th} and a function φ[6]

$$\varphi\left(\sqrt{\frac{a_c}{a_M}}\right) - \varphi\left(\sqrt{\frac{a_{c0}}{a_M}}\right) = \frac{C}{a_M}\left(\frac{g(R)K_{th}}{K_c - \frac{K_{th}}{g(R)}}\right)^n \left(\frac{\sigma_{\max}}{S_{th}}\right)^n N_F$$

$$\text{with} \quad S_{th} = \frac{K_{th}}{Yg(R)\sqrt{a_M}} \tag{3}$$

When $n = 2$, the function φ is expressed as[6]

$$\varphi(x) = 2\ln(x - x_{th}) - \frac{2x}{(x - x_{th})} \quad \text{with} \quad x_{th} = \frac{S_{th}}{\sigma_{\max}} \tag{4}$$

The fatigue behaviour of this material shows scattered results on Wöhler S–N diagrams. For a given load ratio ($R = 0.1$) and a similar number of cycles to failure, the failure stress level may vary by a factor of 1.6 for different specimens subjected to tension (Fig. 2). Two kinds of flaws can be distinguished by SEM analysis, viz. degenerated graphite nodules that

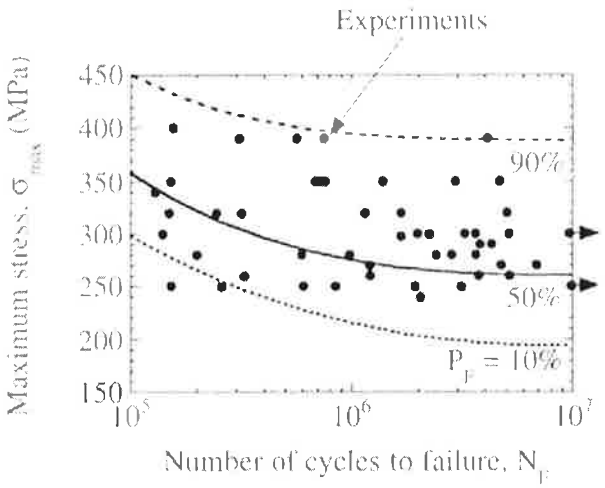

Fig. 2 Fatigue experiments and predicted cumulative failure probabilities in cyclic tension ($R = 0.1$).

are present at the as-cast free surface [Fig. 1(a)], and microshrinkage cavities that exist within the bulk material as well as close to the as-cast free surface [Fig. 1(b)]. These observations justify the use of a probability density function f_0 to describe the flaw size distribution modelled by a beta density[6]

$$f_0(a) = \frac{a^\alpha (a_M - a)^\beta}{B_{\alpha\beta} a_M^{\alpha+\beta+1}} \quad \text{with} \quad B_{\alpha\beta} = \int_0^1 t^\alpha (t-1)^\beta \, dt \tag{5}$$

where α and β are adjustable parameters, and a_M is the maximum flaw size ($0 \leqslant a \leqslant a_M$).

By performing systematic SEM observations of 50 fractured surfaces, the parameters of the flaw size distribution are identified as: $\alpha = 2.3$, $\beta = 18$ and $a_M = 400$ µm, with $V_0 = 340$ mm^3. Consequently, the microshrinkage cavities can be associated with physically short cracks.[7] Secondly, the material parameters of the propagation law can be identified: $C/a_M = 5.9 \times 10^{-5}$, $K_{th}/K_c = 0.33$, $m = 0.59$, $n = 2$, $S_{th} = 105$ MPa, $Y = 2$.[6] The previous material parameters were used to evaluate the tension–compression data obtained on SG cast iron up to 10^7 cycles to failure. A good agreement was found for test results with $R = 0.1$ (see Fig. 2) and $R = -1$.[6] These parameters will be used throughout the present paper, although it is worth noting that corrosive environments could lead to other crack propagation parameters in the vicinity of a free surface[8] and under complex multiaxial stress states.[9] In particular, it is well known that a salt-water environment that exists in off-shore and near-shore structures can seriously affect the fatigue resistance of materials, components and structures. However, this aspect of our work will involve a further study that takes account of the complex loading pattern to which suspension arms are subjected.

The next section is devoted to the definition of the cumulative failure probability associated with the stable propagation of initial cracks under cyclic loading conditions. The initial flaws are modelled as penny-shaped cracks, whose normal is perpendicular to the direction of the local maximum principal stress.

A PROBABILISTIC TREATMENT OF FATIGUE FAILURE

For the sake of simplicity, only the case of constant load levels is discussed. The stress $\sigma_{\max}$ represents the maximum of an equivalent stress (e.g. maximum principal stress) over one loading cycle. We consider an element Ω_0 of volume V_0. It contains initial flaws modelled by penny-shaped cracks of size $2a_0$ and randomly distributed (the initial flaw size distribution is f_0). Under cyclic loading, the initial density f_0 evolves with the number of cycles N to become equal to f_N. The cumulative failure probability P_{F0} depends upon f_N, and is the

probability of finding flaws greater than a_c after N cycles

$$P_{F0} = \int_{a_c}^{+\infty} f_N(a)\,da \quad \text{with} \quad a_c = \left(\frac{K_c}{Y\sigma_{max}}\right)^2 \tag{6}$$

It is assumed that there is no nucleation of flaws during the whole load history: the probability of finding a flaw size equal to a_N after N cycles is the same as the probability of finding an initial flaw a_0. By introducing the initial crack size a_{c0} that becomes critical after N cycles [see Eq. (3)], P_{F0} can be rewritten as[6]

$$P_{F0} = \int_{a_{c0}}^{+\infty} f_0(a)\,da \tag{7}$$

Stating that N_F increases is equivalent to saying that the critical flaw size a_{c0} decreases: more and more critical flaws appear when N_F increases. By noting that crack propagation only occurs when $K_{max}g(R) > K_{th}$, a lower bound to the cumulative failure probability is given by

$$P_{F0} = \int_{a_{th}}^{+\infty} f_0(a)\,da \quad \text{with} \quad a_{th} = \left[\frac{K_{th}}{Yg(R)\sigma_{max}}\right]^2 \tag{8}$$

This case corresponds to the limiting condition $N_F \to +\infty$. For a given stress level σ_{max}, the value of a_{th} denotes the smallest flaw size that is able to propagate. This allows one to compute the fatigue limits associated with the crack propagation law given in the previous section. Equations (7) and (8) show that the most important aspect related to failure is the dimension of the right-hand side tail of the flaw size distribution.

The generalization of the reliability analysis of the volume element Ω_0 to a complex structure Ω of volume V can be obtained by assuming that only flaws initially present within the material cause the failure of the structure. In addition, the interactions between flaws are neglected. In the framework of the weakest link theory,[2] the cumulative failure probability P_F of a structure Ω, for any loading conditions, is related to P_{F0} by

$$P_F = 1 - \exp\left[\frac{1}{V_0}\iiint_{\Omega} \ln(1 - P_{F0})\,dV\right] \tag{9}$$

To be critical, a defect needs to be in the propagation regime (i.e. $K_{max} > K_{th}$) and so the weakest link is not necessarily the largest defect in the structure. Therefore, the knowledge of the whole distribution is important, especially its right-hand side tail. In tension–compression, Eq. (9) becomes

$$P_F = 1 - (1 - P_{F0})^{V/V_0} \tag{10}$$

Thus, according to Eqs (7) and (10), a constant cumulative failure probability P_F is equivalent to considering a constant value a_{c0}, for a given flaw size distribution f_0. This result shows that the crack propagation parameters can be identified from the study of one constant cumulative failure probability (e.g. 50%) in tension–compression.[6]

PREDICTIONS ON SUSPENSION ARMS

Fatigue tests were carried out on suspension arms with a mechanical system which allows one to prescribe biaxial in-plane loading, along two axes X and Y at point C (Fig. 3). These tests were performed for Renault by CETIM. The analysis of the fatigue results again shows important scatter on the F–N diagram (Fig. 4). According to the observations of failure locations, the initiation sites are mainly located in the region indicated in Fig. 3, that is close to the knee joint. By SEM analysis, the same classes of flaws were observed as those in as-cast samples.[6] As a first approximation, we consider that the

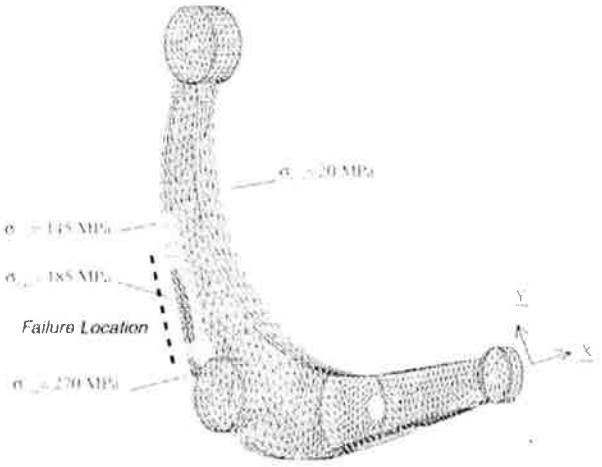

Fig. 3 Contours of maximum principal stress and failure location on suspension arms observed in tests and computations.

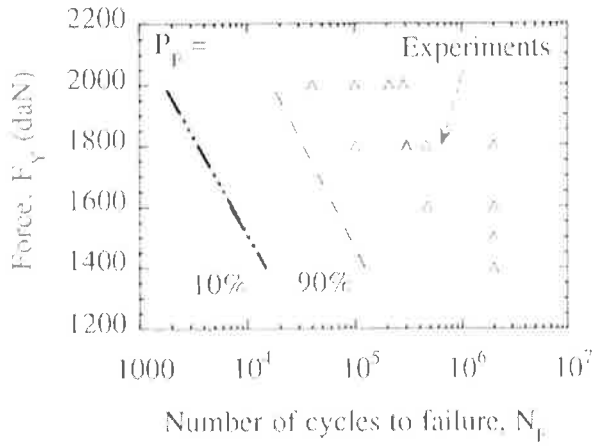

Fig. 4 Predicted constant cumulative failure probabilities compared to experiments carried out on a suspension arm with $R = 0.1$.[5]

relevant flaw size distribution is identical in both cases. Noting that as-cast and double shot-peened suspension arms can be mounted on cars, a physical layer at the free surface is induced by shot-peening. During this process, the degenerated nodules are crushed [Fig. 1(a)] so that the original notch effect they induce disappears.

To assess the predictive capacity of the probabilistic approach, a comparison between fatigue tests carried out on double shot-peened suspension arms and results predicted by the model are now performed. A programme, ASTAR, was developed to evaluate the reliability of components subjected to cyclic loading. This programme allows one to predict the local failure probabilities and the global failure probability of a structure, and integrates the effects of component volume, stress field heterogeneity and flaw size distribution which will be discussed later.

The programme ASTAR is used as a postprocessor of an elastic FE analysis to determine the stress field in structures: at each integration point, the equivalent stress is computed (e.g. maximum principal stress). To this equivalent stress corresponds an initial flaw size a_{c0} for a given number of cycles to failure N_F. This flaw size is computed by integration of Eq. (1) through a Newton method.[10] The failure probability P_{Fe}^j of a finite element j can be calculated by using a Gauss integration of local failure probabilities P_{F0}^i so that P_{Fe}^j depends on the element volume V_e^j, the number n_g of integration points for this element and the weight w_i associated to each integration point

$$\ln(1 - P_{Fe}^j) = \frac{V_e^j}{V_0} \sum_{i=1}^{n_g} [\ln(1 - P_{F0}^i) * w_i] \tag{11}$$

where P_{F0}^i denotes the cumulative failure probability at point i, computed by using Eq. (7). The failure probability of the whole structure P_F is then computed as

$$P_F = 1 - \exp\left[\sum_{j=1}^{n_e} \ln(1 - P_{Fe}^j)\right] \tag{12}$$

where n_e is the number of elements of the structure.

The parameters identified for the flaw distribution and the propagation law constitute the only information needed to run ASTAR. For a given flaw size distribution, the constant cumulative failure probabilities of 10 and 90% are drawn on an σ_Y–N_F plot with $R = 0.1$ (Fig. 4). The experimental fatigue data are reasonably close to the predicted failure probabilities. By inspection of the contours of local cumulative failure probabilities, the most likely sites of failure correspond to those observed experimentally (see Fig. 3). These results confirm that the flaw location with respect to the stress field is of utmost importance. This means that to be critical a defect needs to be subjected to a minimum stress level (such that $\Delta K_{eff} \geq 0$). Moreover, this calculation represents a first pessimistic but reasonable approach for two main reasons: the residual compressive stresses due to the double shot-peening are not taken into account and a single flaw size distribution in the suspension arm (identical to that observed on samples) is considered. In the next section, an endurance limit is defined thanks to an extrapolation to the gigacycle regime by analysing the evolutions of cumulative failure probabilities.

EXTRAPOLATION TO THE GIGACYCLE REGIME

Most fatigue tests performed on specimens to identify Wöhler diagrams are designed to reach failure at a number of cycles close to a maximum of 10 or 20 million. For components, e.g. suspension arms, experiments are often stopped after two million cycles. Hence, the entire endurance limit range is not really well defined.

Extrapolation to 10^9–10^{11} cycles of the results obtained up to 10^7 cycles allows one to determine the error made on the fatigue life in the case of SG cast iron components. The S–N curves that are plotted correspond to different small values of cumulative failure probabilities and are extrapolated from the results given in Ref. [6] and briefly recalled in the previous sections. For a given applied stress σ_{max}, the larger P_{F0}, the larger the number of cycles to failure. To quantify the error for each given P_{F0} (0, 0.01, 0.1, 1 and 10%), the conventional fatigue limit (defined at 10^7 cycles) normalised by the applied stress is plotted versus the number of cycles to failure normalised by 10^7 cycles (Fig. 5). Considering that for the smallest P_{F0} (0%) the error is as small as 3%, it could be rapidly concluded that in the case of the SG cast iron components, performing expensive tests up to 10^9–10^{11} cycles is not necessary. However, it is worth noticing that crack propagation in the

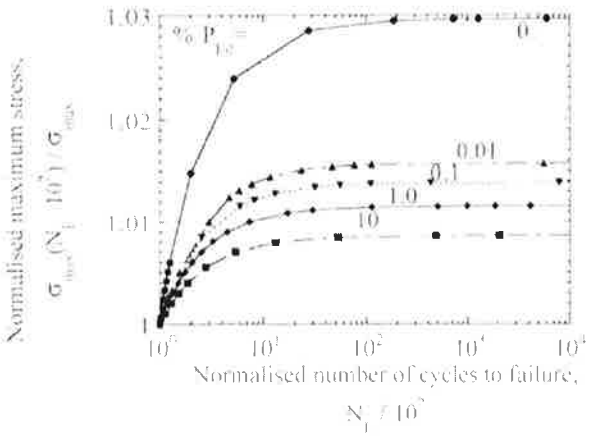

Fig. 5 Change in normalized failure stress with normalized number of cycles to failure for different cumulative failure probabilities.

10^9–10^{11} cycles regime is very close to the non-propagation threshold. The study of the propagation law in this regime shows that the stress intensity factor range is close to zero and that the initial crack size a_{c0} is close to the non-propagation size a_{th} [see Eq. (8)].

The effects on the cumulative failure probability P_F of the flaw size distribution, the volume of the structure and the stress heterogeneity within the structure, respectively (or DVH effects) are discussed in detail in the following section by considering Eqs (8) and (9) in the VHCF regime.

DVH EFFECTS

The flaw size distribution is very important for specimens and also for complex structures in VHCF. The value of the parameters of the flaw size distribution really depends upon the manufacturing process. Endurance maps will show how to treat this problem. Besides, in VHCF, SG cast iron behaves like a brittle material. For such a condition, the volume of the structure is also an important parameter. Lastly, for a complex structure, some volume elements are subjected to more or less high tension while others are subjected to compression. It follows that a study of the stress field heterogeneity is also necessary.

The D effect

For tested specimens, one couple (α,β) (i.e. one flaw size distribution) was determined. However, it is most likely that more than one flaw size distribution is needed to describe the initial state of a complex component, e.g. suspension arm. The present probabilistic model allows one to take account of such a situation.

For a given number of cycles to failure (here $N_F \to +\infty$), and a constant cumulative failure probability P_{F0} (e.g. 0.01%), it is possible to associate a stress level to a couple (α,β) when the load ratio R is chosen. These endurance maps correspond to constant values of the ratio σ_{max}/S_{th} for a given value of P_{F0}. For each stress level, a safety boundary can be drawn. Below a curve representing a given ratio σ_{max}/S_{th}, there is no failure; above it, there is failure when P_{F0} is equal to 0.01% (Fig. 6), as the assumed crack propagation law is deterministic. Hence, the results obtained from fatigue tests on specimens can be extrapolated to industrial components characterized by various flaw size distributions.

To draw this endurance map, an important coefficient is needed: the endurance limit S_{th} for a failure probability $P_{F0} = 0\%$. This last value is directly linked to the threshold stress intensity factor K_{th} and a threshold flaw size a_{th}. The value of S_{th} depends on the material microstructure. It is worth noting that for small flaw sizes (i.e. typically $a_0 \leqslant 500$ μm) the value of K_{th} is independent of the initial flaw size.[4] For larger sizes (i.e. $a_M \geqslant 500$ μm), the value of K_{th} increases with flaw sizes up to a constant value.[4,6] However, in all cases the Paris' regime is obtained[6] (Fig. 7). Therefore, the normalizing stress S_{th} will vary with a_M in general situations.

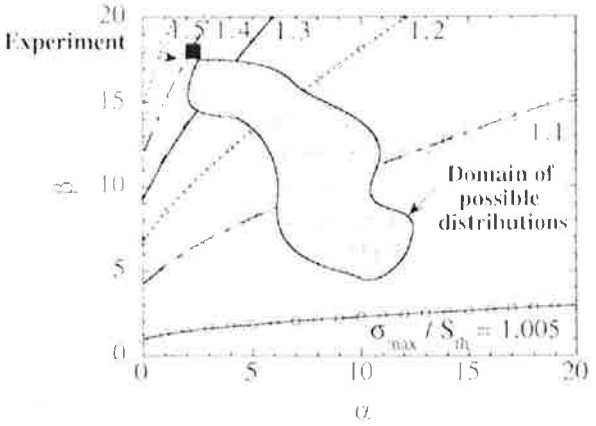

Fig. 6 Endurance map giving different contours of the normalised stress σ_{max}/S_{th} when $P_{F0} = 0.01\%$. The symbol ■ denotes an experiment.

The V effect

In the VHCF regime, the material has a brittle fracture appearance. We can suppose that it is governed by the weakest link assumption.[2] Therefore, the higher the volume, the higher the probability of finding large flaws and the lower the mean failure stress. This effect is well known for concrete and ceramic materials,[11–13] and can be generalised to VHCF of materials whose failure is due to randomly distributed defects.

This result can be shown by considering a crack embedded in a semi-infinite space and subjected to uniaxial cyclic loading. For different diameters of samples (Φ) and a given stress level ($\sigma_{max} = 350$ MPa), Fig. 8

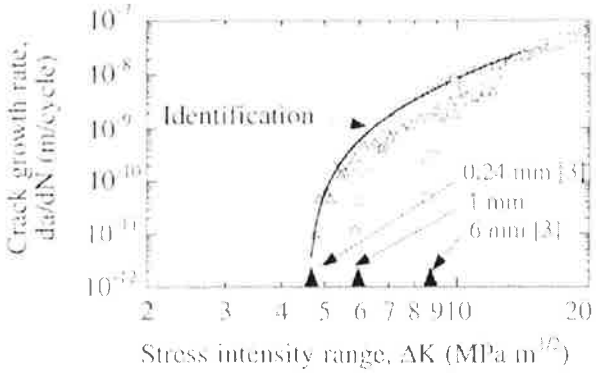

Fig. 7 Evolution of the crack growth rate for different initial flaw sizes a_0.

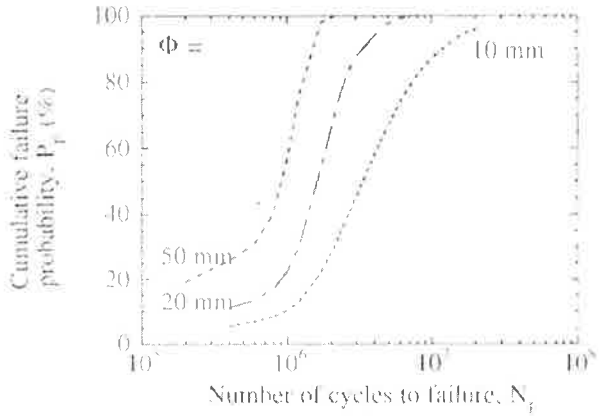

Fig. 8 Volume effect predicted for different sample diameters.

shows that the higher the volume, the higher the failure probabilities for a given number of cycles to failure. Therefore, the geometry, and in particular the volume, are very important features for the fatigue behaviour of complex structures.

The H effect

The effect of the loading pattern on the failure probability is now discussed. Under the condition that $P_{F0} \ll 1$ and the flaw size is bounded by a_M, the beta flaw size distribution can be approximated by

$$f_0(a) \cong \frac{W(a_M - a)^\beta}{a_M^{\beta+1}} \tag{13}$$

The cumulative failure probability of a volume element becomes

$$P_{F0} = \frac{W}{\beta+1}\left[1 - \left(\frac{S_{th}}{\sigma_{max}}\right)^{\beta+1}\right] \tag{14}$$

When the stress level σ_{max} is close to S_{th}, Eq. (14) can be rewritten as

$$P_{F0} = \left[\frac{\langle \sigma_{max} - S_{th}\rangle}{\sigma_0}\right]^{\beta+1}$$
$$\text{with} \quad \sigma_0 = \frac{S_{th}}{2}\left(\frac{W}{\beta+1}\right)^{1/(\beta+1)} \tag{15}$$

Equation (15) corresponds to a three-parameter Weibull law. The parameter β gives the tendency of the initial flaw distribution for large flaws (i.e. $a \cong a_M$). By using Eq. (13), the failure probability of a structure Ω can be written as

$$P_F = 1 - \exp\left[-\frac{H^*_{\beta+1} V}{V_0}\left(\frac{\langle \sigma_F - S_{th}\rangle}{\sigma_0}\right)^{\beta+1}\right],$$
$$\sigma_F = \max_{M \in \Omega}\{\sigma_{max}(M)\} \tag{16}$$

with

$$H^*_{\beta+1} = \frac{1}{V}\iiint_\Omega \frac{\langle \sigma_{max}(M) - S_{th}\rangle^{\beta+1}}{\langle \sigma_F - S_{th}\rangle^{\beta+1}} dV \quad \text{if } \sigma_F > S_{th} \tag{17}$$

where $H^*_{\beta+1}$ is a stress heterogeneity factor which depends upon the load type and load level. The corresponding effective volume V^*_{eff} is given by

$$V^*_{eff} = H^*_{\beta+1} V \tag{18}$$

The effective volume V^*_{eff} is also dependent on the load level. In simple cases, e.g. pure tension, this volume is equal to zero, when $\sigma_F \leqslant S_{th}$, and is equal to V when $\sigma_F > S_{th}$. The previous results will be applied to rotary bending ($R = -1$) of cylindrical samples. In this case, when $\sigma_F > S_{th}$, the parameter $H^*_{\beta+1}$ can be expressed by

$$H^*_{\beta+1} = H_{\beta+1}\left(1 - \frac{S_{th}}{\sigma_F}\right)\left[1 + \frac{S_{th}}{\sigma_F(\beta+2)}\right]$$
$$\text{with } H_{\beta+1} = \frac{2}{\beta+3} \tag{19}$$

The stress heterogeneity factor is a unique parameter characterizing the effect of loading patterns on the failure probability. For a given volume and defect distribution, the more heterogeneous the stress field is, the lower the probability of finding a critical defect in the most loaded area, hence, the lower the stress heterogeneity factor [Eq. (17)] and the failure probability [Eq. (16)].

The suspension arm

The previous results are applied to a suspension arm by using ASTAR (Fig. 5). In Fig. 6, the grey surface represents a schematic of the domain of possible flaw distribution in this structure. By computing the stress

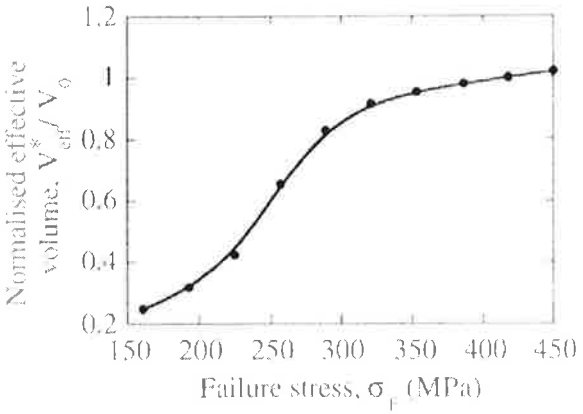

Fig. 9 Change in normalized effective volume V^*_{eff}/V_0 with the failure stress σ_F for a suspension arm with $R = 0.1$.

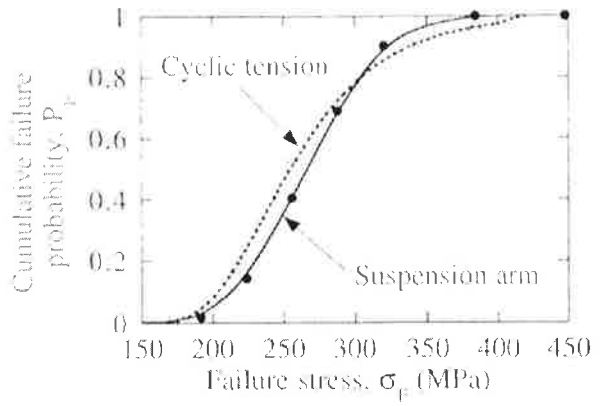

Fig. 10 Comparison of the change in the cumulative failure probability with the failure stress for a suspension arm and a specimen subjected to cyclic tension when $R = 0.1$.

level at each integration point of a FE calculation, it can be checked whether the endurance limits are reached or not. In Fig. 9, the combined V and H effects are taken into account by computing the effective volume for the suspension arm. The value of the effective volume remains close to the volume V_0 of specimens tested in cyclic pure tension ($R = 0.1$). This result explains why, in the VHCF regime, the values of the failure stresses are almost identical in both cases (Fig. 10).

CONCLUSIONS AND PERSPECTIVES

From this study, the main results are:

1 For the case of suspension arms, predictions are conservative. The main reasons for the discrepancies are the following: different flaw populations can be present in the suspension arms when compared to the samples; the residual stresses are not modelled; the effect of the free surface is not accounted for in the vicinity of the as-cast surface where the graphite microstructure is degenerated. When considering shot-peening, the P–N curves will be displaced in the right way because the peening effect allows one to induce compressive residual stresses which delay crack propagation.
2 The extrapolation of lifetimes to 10^9–10^{11} cycles based on results obtained from tests up to 10^7 cycles shows that any error will not be significant even for very small values of the cumulative failure probability.
3 The flaw size distribution, volume and stress heterogeneity (DVH) effects at very high number of cycles to failure (VHCF) are just as significant as in the HCF regime.

To conclude, endurance maps should be established for automatic use in the automotive industry. These maps will help to interpret non-destructive tests, to improve the manufacturing process and the design process itself. Therefore, such a lifing procedure could provide some guidelines on whether to reject or accept a cast component.

However, according to microscopic observations, flaws close to the free surface generally lead to failure. The introduction of microstructural parameters (including shot-peening parameters) in the propagation law appears a natural development to the above-presented probabilistic approach for the prediction of the VHCF and HCF behaviour of cast components.

Acknowledgements

This work was supported by Renault through contract CNRS/1996/014 (H5.24.12) with LMT-Cachan. The authors are grateful to Dr A. S. Béranger and Dr H. Yaacoub Agha for useful discussions.

REFERENCES

1 S.-H. Dai and M. O. Wang (1992) *Reliability Analysis in Engineering Applications*, Van Norstrand Rheinhold, New York, USA.
2 A. M. Freudenthal (1968) Statistical approach to brittle fracture. In: *Fracture* (Edited by H. Liebowitz), Academic Press, New York, USA, Vol. 2, pp. 591–619.
3 F. Hild and D. Marquis (1992) A statistical approach to the rupture of brittle materials. *Eur. J. Mech. A/Solids* **11**, 753–765.
4 P. Clément, J.-P. Angeli and A. Pineau (1984) Short crack behaviour in nodular cast iron. *Fatigue Engng Mater. Struct.* **7**, 251–265.
5 J. Pellas, G. Baudin and M. Robert (1977) Mesure et calcul du seuil de fissuration après surcharge. *Recherche Aérospatiale* **3**, 191–201.
6 H. Yaacoub Agha, A.-S. Béranger, R. Billardon and F. Hild (1998) High-cycle fatigue behaviour of spheroidal graphite cast iron. *Fatigue Fract. Engng Mater. Struct.* **21**, 287–296.
7 K. J. Miller (1993) The two thresholds of fatigue behaviour. *Fatigue Fract. Engng Mater. Struct.* **16**, 931–939.
8 Y. Nadot, N. Raganathan, J. Mendez and A.-S. Béranger (1997) A study of natural cracks initiated on casting defects by crack front marking. *Scripta Mater.* **37**, 549–553.
9 K. J. Miller and R. Akid (1996) The application of microstructural fracture mechanics to various metal surface states. *Proc. R. Soc. Lond. A* **452**, 1411–1432.
10 W. H. Press, S. A. Teukolsky, W. T. Vetterling and B. P. Flannery (1992) *Numerical Recipes in Fortran*, Cambridge University Press, Cambridge, USA.
11 V. Kadlecek and Z. Spleta (1967) Effect of size and shape of test specimens on the direct tensile strength of concrete. *Bull. RILEM* **36**, 175–184.
12 S. L'Hermite (1973) Influence de la dimension absolue sur la résistance de flexion. *Annales ITBTP* **309–310**, 39–41.
13 Y. Katamaya and Y. Hattory (1982) Effects of specimen size on strength of sintered silicon nitride. *C. J. Am. Ceram. Soc.* **65**, C-164–C-165.